Article

Quantifying lithium loss in amorphous silicon thin-film anodes via titration-gas chromatography

Wurigumula Bao, Chengcheng Fang, Diyi Cheng, ..., Weikang Li, Minghao Zhang, Ying Shirley Meng

shmeng@ucsd.edu

Highlights

Li loss in silicon anode is a combination of SEI formation and trapped Li-Si alloy

TGC quantifies the amount of trapped Li-Si alloy

Cryo-TEM reveals the trapped Li-Si alloy intermix with SEI

Growth of SEI is the dominant factor for capacity decay in Si thin-film anodes

Silicon-based anodes for use in lithium-ion batteries are promising, but their fast degradation is not fully understood. Bao et al. apply gas titration chromatography for trapped Li-Si alloy quantification, revealing that interphase-consumed lithium is the primary reason for inferior cycle stability.

Cell Reports
Physical Science

Article

Quantifying lithium loss in amorphous silicon thin-film anodes via titration-gas chromatography

Wurigumula Bao,[1] Chengcheng Fang,[1] Diyi Cheng,[2] Yihui Zhang,[2] Bingyu Lu,[1] Darren H.S. Tan,[1] Ryosuke Shimizu,[1] Bhagath Sreenarayanan,[1] Shuang Bai,[2] Weikang Li,[1] Minghao Zhang,[1] and Ying Shirley Meng[1,2,3,*]

SUMMARY

Silicon with a high theoretical capacity (3,579 mAh/g) is a promising anode candidate for lithium-ion batteries. However, commercialization is still impeded by low Coulombic efficiency, caused by solid electrolyte interphase (SEI) formation and trapped lithium (Li)-silicon (Si) alloy during repeated volume change. Quantifying capacity losses from each factor is crucial to formulate rational design strategies for further improvement. In this work, titration-gas chromatography and cryogenic transmission electron microscopy are applied to characterize the evolution of trapped Li-Si alloy and SEI growth in a silicon thin-film anode. It is found that continuous growth of the SEI is the dominant factor for lithium inventory loss during cycling, with only a marginal increase in trapped Li-Si alloy. This study offers a quantitative approach to differentiate Li in the SEI from trapped Li in Li-Si alloy through a silicon thin-film anode, providing unique insights into identifying critical bottlenecks for developing Si anodes.

INTRODUCTION

Rechargeable lithium-ion batteries (LIBs) are used widely in portable consumer electronics and electric vehicles and show great promise for large-scale grid energy storage. LIBs with high energy density, long cycle life, and low cost have been the main driving forces for developing new electrode materials. Silicon (Si) is a promising candidate for next-generation LIB anode material because of its high specific capacity (lithium $[Li]_{3.75}Si$, 3,579 mAh/g), low alloying potential (0.4 V versus Li^+/Li), and relatively high abundance in the earth's crust.[1–3] However, Si suffers severe volume expansion during the electrochemical lithiation process. This mechanical deformation usually results in more Si surface exposure to the liquid electrolyte, where side reactions occur to form excess solid electrolyte interphase (SEI) with Li inventory loss.[4,5] Extensive studies have proposed that SEI properties have a critical effect on Si anode cycling performance. On one hand, it is believed that inorganic SEI species, such as lithium fluoride (LiF) and Li_2O, contribute to better cycling stability because the ionic bonds can facilitate hopping-type transport.[6] Inorganic SEI components can also adapt to the plastic deformation caused by volume expansion because of their high Young's modulus and high interfacial energy (low adhesion) with Li-Si alloy.[4,7] On the other hand, the Si SEI is a group of Li compounds, including Li_2CO_3, LiF, Li_2O, Li_xSiO_y, dilithium ethylene glycol dicarbonate (Li_2EDC), and ROLi (where R depends on the solvent).[8–11] Excess formation of Li-containing SEI species consumes limited active Li ions in a full cell, reducing the reversible capacity during cycling.[12]

[1]Department of NanoEngineering, University of California, San Diego, La Jolla, CA 92093, USA

[2]Materials Science and Engineering, University of California, San Diego, La Jolla, CA 92093, USA

[3]Lead contact

*Correspondence: shmeng@ucsd.edu

https://doi.org/10.1016/j.xcrp.2021.100597
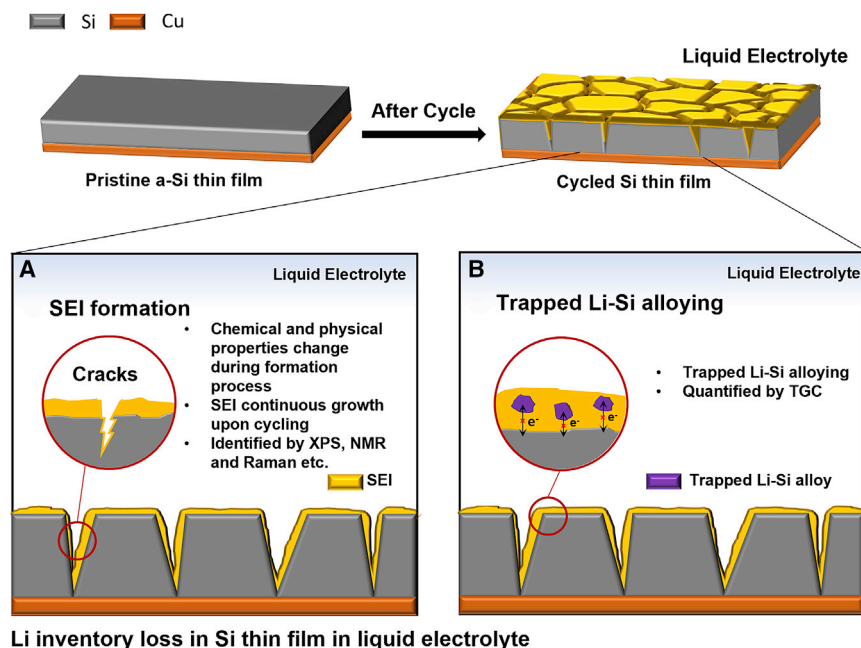
Li inventory loss in Si thin film in liquid electrolyte

Figure 1. Schematic of two types of active Li loss in silicon anodes
(A) SEI formation.
(B) Trapped Li-Si alloy.

Multiscale characterizations have been employed to investigate continuous SEI growth for Si anodes.[13] Veith et al.[14] applied *in situ* neutron reflectometry (NR) to identify SEI thickness on Si thin-film anodes, revealing SEI thickening upon lithiation and SEI thinning with delithiation. Zheng et al.[4] reported the same findings via atomic force microscopy (AFM). Tip-enhanced Raman spectroscopy (TERS)[15] and scanning spreading resistance microscopy (SSRM)[16] have been applied to demonstrate that SEI chemical properties changed during cycling because of significant volume expansion. Qualitative analysis has been carried out to study the Si SEI's dynamic nature, but a quantitative understanding of SEI growth during cycling and its correlation to Li loss remained unclear.

Volume expansion not only introduces excess SEI formation but also leads to loss of electrical contact between the active materials and the conducting network.[17] Additionally, growth of the SEI and the increase in electrode tortuosity during cycling blocks diffusion of Li ions and the electron conduction channels.[18] As a result, part of the Li is trapped irreversibly within the Si electrode.[19] However, lack of proper characterization has hampered quantification of the remaining Li in Si anodes. Two types of Li inventory loss are shown in Figure 1: continuous formation of the SEI during cycling and trapped Li in Li-Si alloy because of kinetic hindrance. Quantifying Li loss caused by different factors is thus key to elucidate the degradation mechanism of Si anodes.

Here we quantitatively studied the SEI formation process through an amorphous Si thin film to prevent binder and conductive carbon interference in data interpretation.[20,21] In addition, the volume expansion of an amorphous Si thin film is isotropic without two-phase lithiation conversion.[22] Thus, the aim of this research is maximally simplified. In this work, we set up a method based on titration-gas chromatography (TGC) to quantify Li loss in Li-Si alloy. The primary chemical mechanism is that the

Cell Reports
Physical Science
Article

CellPress
OPEN ACCESS

Li-Si alloy can react with the inert protic solvent and produce hydrogen (H_2) but the SEI components cannot.[23] This method allowed us to quantitatively distinguish the loss of active Li consumed by SEI formation and the trapped Li-Si alloy caused by the kinetic limitation. We investigated SEI evolution in the first cycle, and SEI growth in subsequent cycles was studied thoroughly under controlled electrochemical conditions. The results show that SEI formation starts at 0.5 V and stops growing when the lithiation voltage reaches 0.24 V (versus Li^+/Li) at the first cycle. This indicates that the SEI does not grow linearly in a Si thin-film anode during the whole lithiation process. Upon subsequent cycling, accumulation of SEI is the dominant factor for Li loss, with only a marginal increase in trapped Li-Si alloy. These findings provide a unique understanding of SEI growth and evolution in amorphous Si thin films and quantitative information about Li inventory loss caused by different factors. The developed workflow can be applied widely to study Li inventory loss for other conversion or alloy-type anode materials.

RESULTS AND DISCUSSION

Solvent screening for the TGC methodology

To develop the TGC method for Li quantification in Li-Si alloy, we first explored the reaction mechanisms between Li-Si alloy and protic solutions (water/ethanol). The chemical reaction formula is

$$2Li_xSi\ (s) + 2xH^+\ (aq.) = 2xLi^+\ (aq.) + 2\ Si\ (s) + xH_2 \qquad \text{(Equation 1)}$$
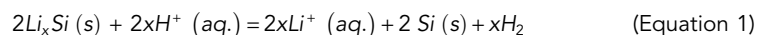
Pure Si is one of the reaction products, and it undergoes multi-step reactions with H_2O to generate H_2 gas.[24] Therefore, a suitable solvent needs to meet the following criteria: (1) chemically inert with Si and only reacting with Li-Si alloy to generate H_2 gas and (2) chemically inert with the SEI components with no H_2 generation. Starting with three common solvents, H_2O, H_2SO_4, and C_2H_5OH (EtOH), a controlled TGC experiment was conducted with fully lithiated Si thin-film electrodes and nano-Si with/without LiF mixtures. Figure 2B shows that the amount of H_2 generated from the lithiated Si thin film (lithiated to 0.01 V versus Li^+/Li) varies when using different titration solvents. The theoretical amount of H_2 calculated based on Equation 1 is shown as a green horizontal line for reference. The amounts of generated H_2 when using H_2SO_4 and EtOH are close to the theoretical value (see details in Figure S2). The excess H_2 amount for H_2O solvent shows that H_2O undergoes side reactions with the lithiated Si anode, as discussed above. Another control experiment was conducted using nano-Si powder to confirm this observation; the related discussion can be found in Figure S3 and Note S1. Figure 2C shows that H_2 is generated from bare nano-Si when mixing with H_2O, but no H_2 can be detected when using H_2SO_4 or EtOH solvents. Previous studies reported that concentrated alkaline solutions accelerate Si oxidation to produce H_2.[25] In addition to Li-Si alloy, the solubility and reactivity of SEI components in the three solvents also has to be considered (SEI components and results are summarized in Figure S4 and Table S2). Most of the SEI components are stable with selected solvents except for LiF. Figure 2D shows that nano-Si mixed with LiF reacts and generates H_2 when H_2SO_4 solvent is used. This is due to HF(Hydrofluoric acid) formation from LiF in acidic environments, which further reacts with Si to yield H_2.[26] Neither H_2O nor H_2SO_4 solution is suitable for TGC experiments for quantification of Li in Li-Si alloy. EtOH as a mild protic solvent is chemically stable with Si SEI components. EtOH can also react with Li-Si alloy to generate H_2 for Li quantification. Therefore it was chosen as the solvent for the subsequent TGC study.

The total amount of Li within the Si anode equals the sum of the Li amount in the SEI (Li^+) and Li-Si alloy because some Li reacts with Si to form Li-Si alloy, whereas some is
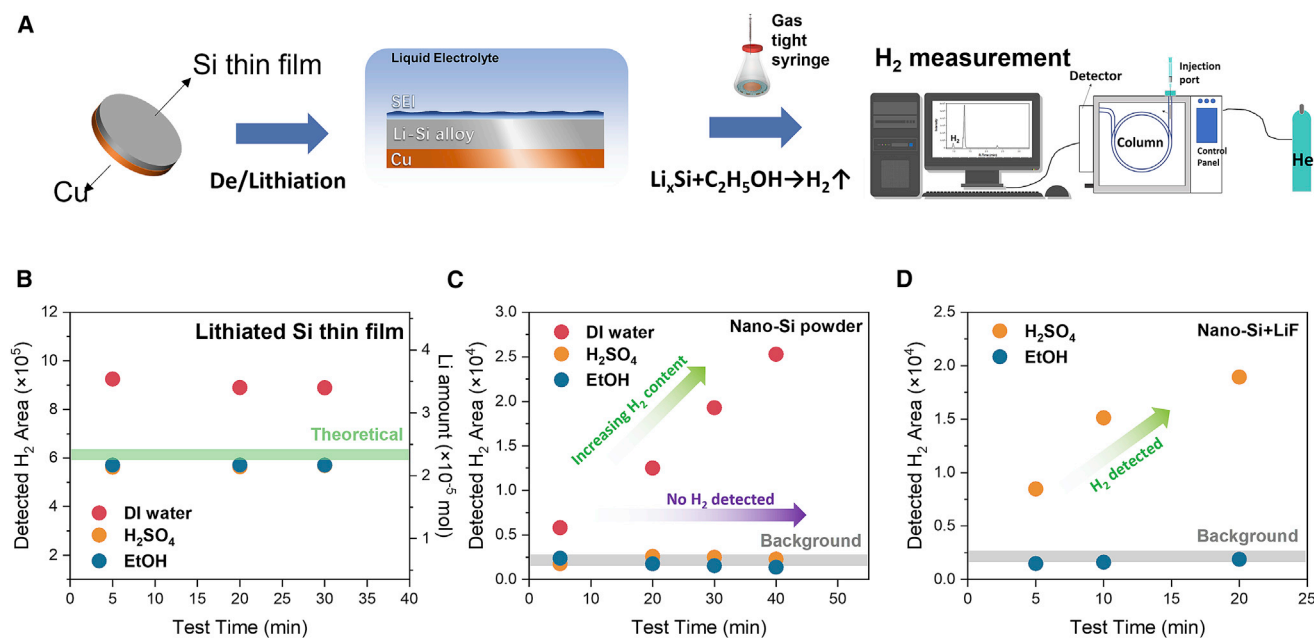
CellPress
OPEN ACCESS

Figure 2. TGC solvent screening for the Si anode
(A) Schematic of the titration-gas chromatography (TGC) workflow conducted on the Si thin film.
(B–D) Titration solvent selection for TGC measurements of (B) lithiated Si thin film, (C) nano-Si, and (D) nano-Si + LiF.

consumed irreversibly to form the SEI during lithiation. The Li content in Li-Si alloy can be determined by the TGC method. The Li content in the SEI can be calculated using the total Li amount obtained from electrochemical testing. To verify that the Li-Si alloy is fully reacted with the titration solvent, inductively coupled plasma mass spectrometry (ICP-MS) was conducted on Si thin-film samples after titration with EtOH. No additional Li ions were detected in the filtered solution, indicating that the EtOH solvent fully reacted with the Li-Si alloy samples (Figure S5; Table S3; Note S2).

Quantification and qualification of first-cycle Li loss in the Si thin-film anode

Different lithiation/delithiation states were selected by controlling the Li | Si half-cell cutoff voltage or capacity to quantify Li-Si alloy by the TGC method (see more details in Table S4). Figure 3A displays the electrochemical discharge profiles of the lithiation processes with the corresponding TGC results. From the electrochemical data, at point of lithiation (PL) 1 (0.5 V), the lithiation capacity is 0.0045 mAh. However, no H_2 was detected at 0.5 V (PL 1) when the lithiation reaction starts, indicating that SEI formation occurs before the Li-Si alloying reaction. H_2 gas was detected from 0.35 V versus Li^+/Li (PL 3), suggesting that the beginning of the alloying reaction is between 0.4 V and 0.35 V versus Li^+/Li (PL 2 and PL 3). The Li-Si alloy and SEI amounts increase when they reached potential for PL 4 and PL 5. The SEI stops growing after 0.24 V versus Li^+/Li (PL 5) and remains the same until 0.01 V versus Li^+/Li (PL 8). Completion of SEI growth demonstrated that new surfaces would no longer be formed at the initial lithiation process of the Si thin-film anode.

The electrodes were charged to different delithiation states after being discharged to 0.01 V (versus Li^+/Li) (Figure 3B). From PD 1 to PD 5, Li should be delithiated gradually from the Li-Si alloy. The TGC results reflect the process clearly, showing a decreasing trend of Li-Si alloy amount during the delithiation process. However, the SEI amount has no noticeable change during the delithiation process. At the
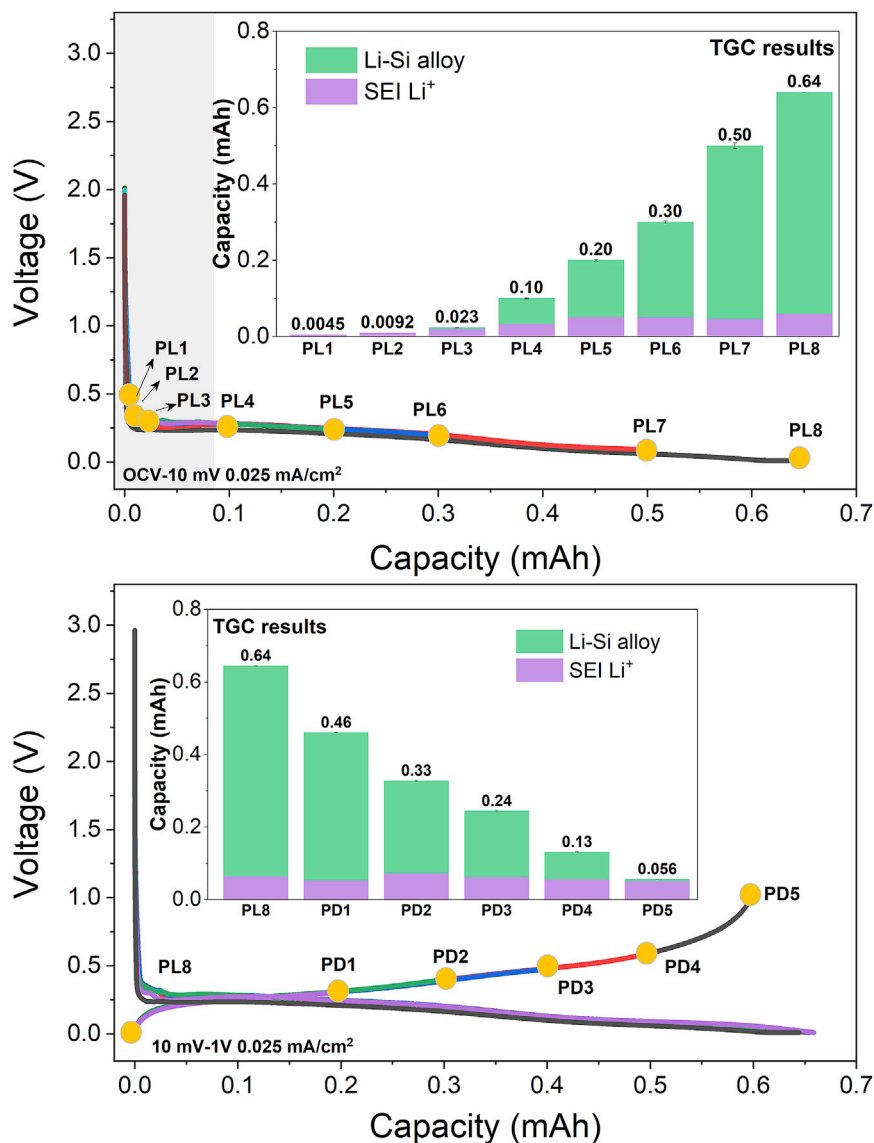
CellPress
OPEN ACCESS

Figure 3. Li quantification in the Si anode at the first cycle
(A) Charge and discharge profiles of Si thin film and TCG results of the lithiation process with different cutoff voltages.
(B) Delithiation process with different cutoff capacities. PL, point of lithiation; PD, point of delithiation. Error Bars Representing the Standard Errors

delithiated state of PD 6 (1 V versus Li^+/Li), H_2 gas was still detectable, indicating the presence of trapped Li-Si alloy. Thus, Li loss during the first cycle in the Si thin-film anode comes from the SEI and the trapped Li-Si alloy. Specifically, 91% of the capacity loss in the first cycle is due to SEI formation, and the remaining 9% is due to the trapped Li in the Li-Si alloy.

Cryo-transmission electron microscopy (TEM) coupled with cryogenic lift-out methodology was applied to investigate the trapped Li-Si alloy after the first cycle. Cryogenic condition is critical here because lithiated Si is highly sensitive to the electron beam, inducing sample damage at room temperature.[27] In Figure 4A, the pristine Si thin-film sample is in the middle layer of the Pt (top) and Cu current collector
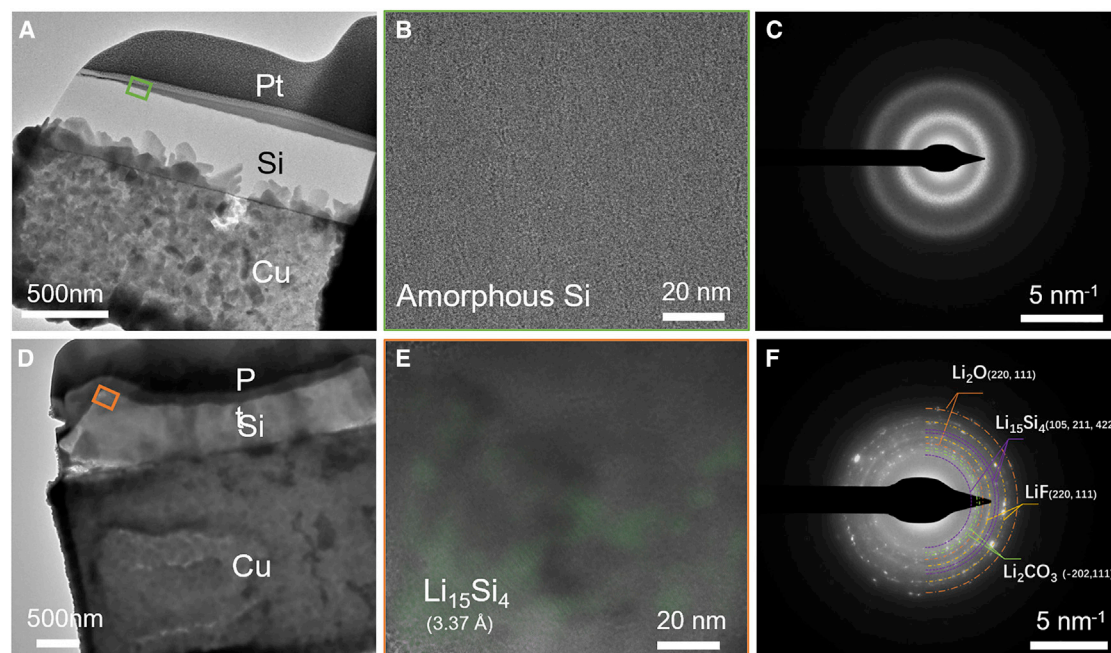
Figure 4. Nanostructures of trapped Li-Si alloy in the Si thin film anode after the first cycle by cryo-TEM
(A and D) TEM images for (A) pristine and (D) cycled Si thin-film anode samples.
(B, C, E, and F) HRTEM images of (B) pristine and (C) cycled Si thin-film electrode and (C and F) SAED patterns corresponding to (B) and (E).

(bottom). The as-deposited Si thin film is 500 nm thick with a negligible native oxide layer on the surface, confirmed by EDS mapping of Pt, Si, O, and Cu in Figure S6A. No crystal lattice was identified in the pristine Si thin-film sample in the high-resolution TEM (HRTEM) image (Figure 4B) in the region highlighted by the green squares in Figure 4A. The selected area electron diffraction (SAED) in Figure 5C shows halo features, demonstrating the amorphous nature of the deposited Si sample. After the first cycle, the electrode thickness increased to 530 nm, and a 20-nm-thick SEI was formed on the surface. The SEI layer can be depicted by the uniform elemental distribution of O and F on the surface, as shown in Figure S6B. The region highlighted by the orange frame in Figure 4D was analyzed further by HRTEM and SAED (Figures 4E and 4F). It can be confirmed from the SAED pattern in Figure 4E that the SEI is composed of polycrystalline and amorphous species, including Li_2O, Li_2CO_3, and LiF.[28–30] In addition, the (1 0 5), (2 1 1), and (4 2 2) crystallographic planes of $Li_{15}Si_4$ are also found in the SAED pattern. The presence of $Li_{15}Si_4$ is consistent with the TGC results showing that trapped Li-Si alloy exists in the Si thin-film anode. The HRTEM image (Figure 4E) also shows that the trapped Li-Si alloy regions intermixed with the SEI. This suggests that blocking the electron pathway can induce formation of trapped Li-Si alloy from the SEI during the delithiation process.

Quantifying extended cycles of Li loss in the Si thin-film anode
We further investigated the SEI and trapped Li-Si alloy amounts during extended cycles. The charge-discharge profiles and cycling performance of Si thin-film half cells are shown in Figures 5A and 5B. The current density used in the first cycle was 0.025 mA/cm^2 and then switched to 0.10 mA/cm^2 for subsequent cycles. The initial lithiation capacity was 0.42 mAh/cm^2 with an initial Coulombic efficiency of 93%. No capacity decay was observed during the initial 30 cycles, whereas severe degradation occurs with decreased Coulombic efficiency thereafter. The TGC measurements
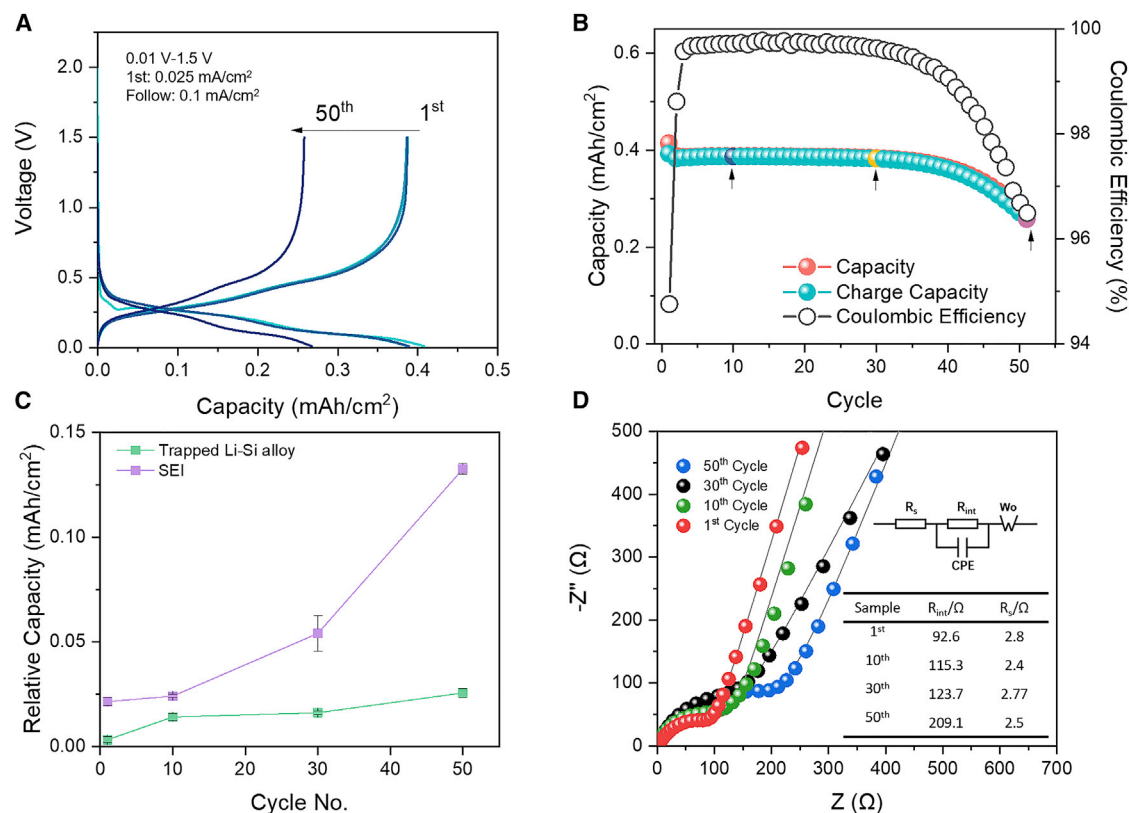
Figure 5. Li quantification in the Si anode at following cycles

(A and B) Charge/discharge voltage profiles (A) and cycling performance (B) of Si thin film in half-cell.

(C) TGC results of the Si thin film at different cycles. Error bars represent the standard error.

(D) EIS Nyquist plots of an Si thin-film half cell at different cycles.

were conducted at cycles 10, 30, and 50 to pinpoint the degradation mechanism. The total capacity loss, amount of SEI, and trapped Li-Si alloy were obtained by Equation 2:

$$\sum_1^N Q_{Capacity\ loss} = \sum_1^N Q_{SEI} + \sum_1^N Q_{Trapped\ Li},$$ (Equation 2)

where N represents the cycle number and $Q_{capacity\ loss}$, Q_{SEI}, and $Q_{trapped\ Li}$ refer to capacity loss from each component at each cycle. As shown in Figure 5C, the primary capacity loss during cycling is continuous formation of the SEI, which accumulates much faster than trapped Li-Si alloy. Electrochemical impedance spectroscopy (EIS) was conducted to explore the interphase impedance changes during extended cycles. Figure 5D shows a correlation between interphase impedance and SEI growth. The interphase impedance is 92.6 Ω at the first cycle and increases to 115.3 Ω, 123.7 Ω, and 209.1 Ω over 10, 30, and 50 cycles respectively, indicating that the SEI changed upon cycling.

Cross-section images were captured using cryogenic focused ion beam scanning electron microscopy (FIB-SEM). Figure 6A shows a dense and flat 500-nm-thick Si thin film as the pristine state, but cracks appear on the surface because of volume change after the first cycle. After 10 and 30 cycles, the surface starts to pulverize into small fragments. Considering that the specific capacity barely changes within 30 cycles, the total amount of active material should not be affected by those cracks.
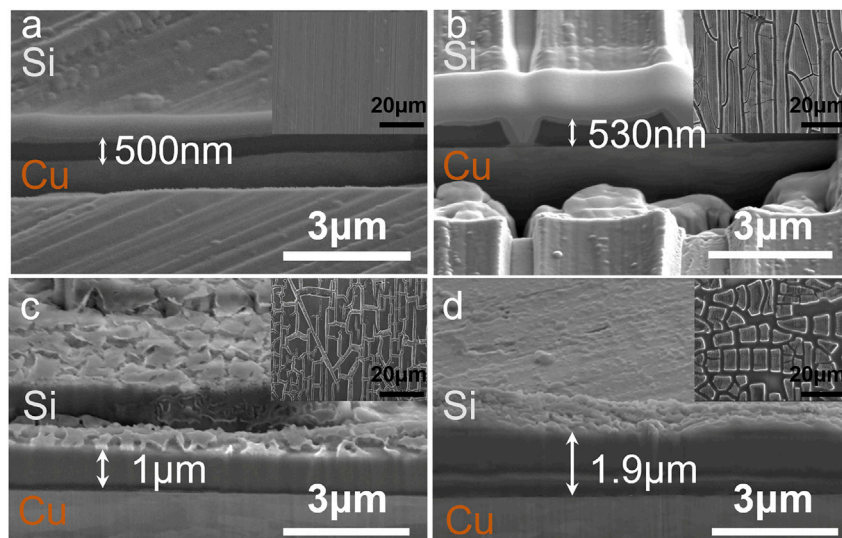
CellPress
OPEN ACCESS

Cell Reports
Physical Science
Article

Figure 6. Cryo-FIB-SEM for cross-section and top-view surfaces of the Si thin-film electrode
(A) Pristine.
(B) After 1 cycle.
(C) After 10 cycles.
(D) After 30 cycles.

As shown in Figure 6, the electrode thickness increases after the cycling. Consequently, these cracks drastically increase the surface area of exposed Si and lead to continuous SEI growth.

The TGC results show that the initial SEI growth stops after the first lithiation to 0.24 V. It is possible that the majority of the capacity is achieved with a voltage lower than 0.24 V, where no SEI grows. This indicates that voltage control should be effective for improving Si anode cycling. The upper cutoff voltage can be lowered to validate this hypothesis. Figures 7A and 7B show the cycling performance of the Si thin film in half cells with different upper cutoff voltages, including 0.6 V, 0.8 V, and 1.5 V. The initial Coulombic efficiencies are 77.96%, 85.37%, and 94.76%, respectively. The decreased ICE is due to incomplete delithiation because of limitation from the upper cutoff voltage. The average CEs from the second and 50th cycles for 0.6 V, 0.8 V, and 1.5 V cutoff are 99.74%, 99.41%, and 99.19%, and the capacity retention values are 96.67%, 86.53%, 72.26%, respectively. The cycle stability and Coulombic efficiencies are improved significantly with the decrease in delithiation potential. The TGC results also show (Figure S7) that the amounts of SEI and trapped Li-Si alloy were reduced in 0.6-V cells compared with 1.5-V cells. The decrease in the total SEI amount reduces the chance of the Li-Si alloy being isolated by the SEI, reducing the amount of trapped Li-Si alloy. The percentage of used Si anode controlled by the cutoff voltage can be mimicked in a full-cell setup. Changing the capacity ratio between the negative and positive electrodes (N/P ratio) would have a similar effect as the voltage control.

Correlating the amount of Li inventory loss with micro- and nanostructures, we propose a mechanism of Li loss in the amorphous Si thin-film anode. The dominant reason for Li inventory loss is formation of the SEI: the electrolyte decomposes on the electrode surface to form organic and inorganic Li-containing compounds. Despite the conventional understanding that large volume changes in Si anodes during the lithiation process result in continuous SEI growth, the quantitative analysis
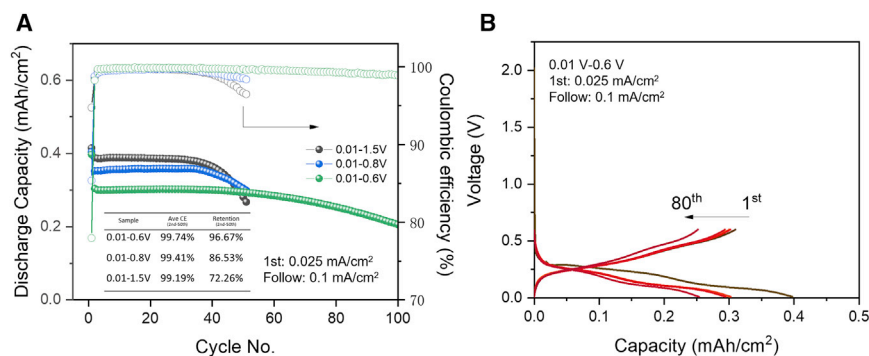
Figure 7. Cycling performance with different upper cutoff voltages
(A and B) Charge/discharge voltage profiles (A) and cycle performance (B) of the Si thin film at voltage ranges of 0.01–0.6 V, 0.01–0.8 V, and 0.01–1.5 V.

conducted in this work shows no clear relationship between volume expansion and SEI growth. The SEI stops growing after 0.24 V during the initial lithiation process. An increase in the SEI during the subsequent cycling is likely due to formation of cracks during the delithiation process, which increases the specific surface area of the electrode. Therefore, controlling the delithiation process and its corresponding volume change is critical for achieving improved cycling stability. The second reason for Li inventory loss is formation of trapped Li-Si alloy, which was identified by TGC and cryo-TEM results. Trapped Li-Si alloy during cycling contributes to capacity loss. Crystalline $Li_{15}Si_4$ is the most stable phase of Li-Si alloy at room temperature, and it is derived from amorphous Li_xSi after lithiation to 0.01 V (versus Li/Li$^+$).[31] The cryo-TEM image shows that trapped $Li_{15}Si_4$ is encapsulated by the insulating SEI, leading to loss of electron conduction pathways. This indicates that the amount of trapped Li-Si alloy can be reduced by controlling the amount of SEI formed. The TGC results in Figure S7 demonstrate that a more controlled SEI can reduce the trapped Li-Si alloy. Li inventory loss in amorphous Si thin-film anodes consists of the SEI and trapped Li-Si alloy. The SEI is the primary reason for capacity decay.

Here, a TGC method was designed to investigate Li inventory loss in Si thin-film anodes. The choice of titration solvent is crucial for accurate quantification, and the chemical properties of the Li-Si alloy and SEI components need to be considered carefully. Ethanol was selected as the titration solvent because only the Li-Si alloy can be titrated to generate H_2, rather than other side reactions induced by common SEI components. With the optimized TGC method, we demonstrated that inventory Li loss in Si thin-film anodes is mainly caused by continuous SEI formation along with cycling. For the first lithiation process, SEI formation stops when the voltage reaches 0.24 V, whereas the SEI amount shows negligible changes during the first delithiation process. Trapped Li-Si alloy can be detected after delithiation to 1.5 V by TGC and cryo-TEM and is intermixed with the insulating SEI components. The trapped Li-Si alloy and SEI grow with cycling, but the SEI consumes most of the Li inventory. We believe that the cracks induced by the volume change increase the surface area of Si so that more SEI will be formed with trapped Li-Si alloy. Controlling the upper cutoff voltage can mitigate SEI formation, resulting in less trapped Li-Si alloy and better cycling stability. We validate the TGC method in Si thin-film anodes and increase our understanding of the Si anode degradation mechanism. We believe that this approach can be applied universally in Si-based or other alloy-type anode material to accelerate development of high-energy-density secondary batteries.

EXPERIMENTAL PROCEDURES

Resource availability

Lead contact
Further information and requests for resources and reagents should be directed to and will be fulfilled by the lead contact, Ying Shirley Meng (shmeng@ucsd.edu).

Materials availability
This study did not generate new unique reagents.

Data and code availability

The authors declare that data supporting the results of this study are available in the paper and supplemental information. All other data are available from the lead contact upon reasonable request.

Preparation of the Si thin film

A Si thin film with 500-nm thickness was used as the anode in this study. The film was deposited on Cu foil (10 μm, MTI) by magnetron sputter deposition with an RF power supply using the Si (99.99%) target from Kurt J. Lesker (3 inches in diameter and 0.125 inches in thickness). The deposition was conducted in a Discovery 18 sputtering system made by Denton Vacuum. A base pressure of 8×10^{-7} torr was achieved before deposition. An argon gas pressure of 5×10^{-3} torr and a power level of 350 W were applied during deposition. The density of the Si thin film was around 2.2 g/cm^3, measured by quartz crystal microbalance (QCM). The morphology is shown in Figure S1. The titrants included DI H_2O, 0.07 M H_2SO_4 solution (diluted from 18.4 M H_2SO_4, Fisher Chemical), and ethanol (200-proof anhydrous ethanol, Koptec, 99.9% or greater). Nano-sized Si powder (nano-Si, <50 nm, Alfa Aesar) and LiF (≥99.99% trace metals basis, Sigma-Aldrich) were used to demonstrate the reaction between Si and solvent.

Electrochemical measurements

The Si thin film with a diameter of 0.55 inches as the working electrode was assembled into a 2032-type coin cell in an Ar-filled glove box. Li metal (1 mm thick, 0.5 inches in diameter) was employed as the counter electrode. The electrolyte was 1 mol/L $LiPF_6$ dissolved in ethylene carbonate (EC):dimethyl carbonate (DMC) (1:1, v/v) with 10% of fluoroethylene carbonate (FEC), and the electrolyte amount was fixed as 75 μL/cell. The half cell was cycled between 10 mV and 1.5 V at room temperature at a current density of 0.025 mA/cm^2 during the first cycle and 0.1 mA/cm^2 for subsequent cycles using a Neware battery tester. We controlled different lithiation states for TGC samples during lithiation by limiting the cutoff voltage or the cutoff capacity. Characterization of electrochemical impedance was performed using a BioLogic SP-150 workstation under OCV with 1 MHz–10 mHz as the frequency range.

TGC

The TGC experiments were performed using a Shimadzu GC-2010 Plus Tracera equipped with a barrier ionization discharge (BID) detector. The split temperature was kept at 200°C with a split ratio of 2.5 (split vent flow, 20.58 mL/min; column gas flow, 8.22 mL/min; purge flow, 0.5 mL/min). The column temperature (RT-Msieve 5A, 0.53 mm) was kept at 40°C, and the BID detector was held at 235°C. Helium (99.9999%) was used as the carrier gas, and the BID detector gas flow rate was 50 mL/min. After cycling to the designed condition, the cycled cells were dissembled in the Ar-filled glove box, and then the cycled electrode was transferred into a glass vial with a rubber septum for air-tight sealing. The whole

Cell Reports
Physical Science
Article

process was conducted in the glove box to prevent air exposure. Then the vials were transferred for titrate injection. The generated gases after titration were injected into the machine via a 50-μL gas-tight Hamilton syringe, as shown in Figure 2A. The related calibration procedure can be found in the supplemental experimental procedures and Table S1.

ICP-MS
ICP-MS (iCAP RQ, Thermo Fisher Scientific) was applied to quantify Li amount. The sample was soaked in a 0.5-M H_2SO_4 solution overnight for fully dissolve. Then the supernatant was collected and diluted with matrix solution for ICP.

X-ray photoelectron spectroscopy
X-ray photoelectron spectroscopy (XPS) was conducted on a Kratos AXIS-Supra, using an Al target as the X-ray source under 10^{-9} torr pressure. The cycled electrodes for XPS tests were rinsed with DMC and then transferred to a nitrogen-filled glove box directly connected to the chamber without air exposure. Survey scans were performed with a step size of 1.0 eV, followed by a fine scan with 0.1-eV resolution. The spectra were analyzed by CasaXPS software to differentiate chemical species.

FIB-SEM
FIB-SEM was conducted on an FEI Scios dual-beam microscope; Si thin-film cells after cycling were disassembled in an Ar-filled glove box. The samples were transferred to the FIB chamber without any exposure to air. The electron beam operating voltage was 5 kV, and the stage was cooled with liquid nitrogen to −180°C or below. Sample cross-sections were exposed using a 1-nA ion beam current and cleaned at 0.1 nA.

Cryogenic lift-out methodology and cryo-TEM
The Cryo-FIB preparation process was performed as described above. The Pt was deposited for surface protection from the ion beam and connected lamella with the tungsten probe for lamella lift-out and mounting; more details can be found in our previous work.[32] The lift-out sample was removed from the FIB chamber under a vacuum using an air-free quick loader (FEI), and the sample was transferred in an Ar-filled glove box. A TEM cryo-holder (Gatan) was used to load the sample; TEM grids were immersed in liquid nitrogen and then mounted onto the holder via a cryo-transfer workstation. The whole TEM sample preparation and transfer process prevented sample contact with air at room temperature. Scanning transmission electron microscopy/energy dispersive X-ray spectroscopy (STEM/EDS) mapping, TEM images, and SAED patterns were conducted on a JEOL JEM-2800F transmission electron microscope equipped with a Gatan Oneview camera operated at 200 kV.

SUPPLEMENTAL INFORMATION
Supplemental information can be found online at https://doi.org/10.1016/j.xcrp.2021.100597.

CellPress
OPEN ACCESS

Cell Reports
Physical Science
Article

AUTHOR CONTRIBUTIONS

DECLARATION OF INTERESTS

REFERENCES

1. Shobukawa, H., Shin, J., Alvarado, J., Rustomji, C.S., and Meng, Y.S. (2016). Electrochemical reaction and surface chemistry for performance enhancement of a Si composite anode using a bis(fluorosulfonyl)imide-based ionic liquid. J. Mater. Chem. A Mater. Energy Sustain. 4, 15117–15125.

2. Ashuri, M., He, Q., and Shaw, L.L. (2016). Silicon as a potential anode material for Li-ion batteries: where size, geometry and structure matter. Nanoscale 8, 74–103.

3. Zuo, X., Zhu, J., Mueller-Buschbaum, P., and Cheng, Y.-J. (2017). Silicon based lithium-ion battery anodes: A chronicle perspective review. Nano Energy 31, 113–143.

4. Zheng, J., Zheng, H., Wang, R., Ben, L., Lu, W., Chen, L., Chen, L., and Li, H. (2014). 3D visualization of inhomogeneous multi-layered structure and Young's modulus of the solid electrolyte interphase (SEI) on silicon anodes for lithium ion batteries. Phys. Chem. Chem. Phys. 16, 13229–13238.

5. Dupré, N., Moreau, P., De Vito, E., Quazuguel, L., Boniface, M., Bordes, A., Rudisch, C., Bayle-Guillemaud, P., and Guyomard, D. (2016). Multiprobe study of the solid electrolyte interphase on silicon-based electrodes in full-cell configuration. Chem. Mater. 28, 2557–2572.

6. Schroder, K., Alvarado, J., Yersak, T.A., Li, J., Dudney, N., Webb, L.J., Meng, Y.S., and Stevenson, K.J. (2015). The effect of fluoroethylene carbonate as an additive on the solid electrolyte interphase on silicon lithium-ion electrodes. Chem. Mater. 27, 5531–5542.

7. Chen, J., Fan, X., Li, Q., Yang, H., Khoshi, M.R., Xu, Y., Hwang, S., Chen, L., Ji, X., Yang, C., and He, H. (2020). Electrolyte design for LiF-rich solid–electrolyte interfaces to enable high-performance microsized alloy anodes for batteries. Nat. Energy 5, 386–397.

8. Cao, C., Abate, I.I., Sivonxay, E., Shyam, B., Jia, C., Moritz, B., Devereaux, T.P., Persson, K.A., Steinrück, H.-G., and Toney, M.F. (2019). Solid Electrolyte Interphase on Native Oxide-Terminated Silicon Anodes for Li-Ion Batteries. Joule 3, 762–781.

9. Yoon, T., Milien, M.S., Parimalam, B.S., and Lucht, B.L. (2017). Thermal decomposition of the solid electrolyte interphase (SEI) on silicon electrodes for lithium ion batteries. Chem. Mater. 29, 3237–3245.

10. Breitung, B., Baumann, P., Sommer, H., Janek, J., and Brezesinski, T. (2016). In situ and operando atomic force microscopy of high-capacity nano-silicon based electrodes for lithium-ion batteries. Nanoscale 8, 14048–14056.

11. Young, B.T., Heskett, D.R., Nguyen, C.C., Nie, M., Woicik, J.C., and Lucht, B.L. (2015). Hard X-ray photoelectron spectroscopy (HAXPES) investigation of the silicon solid electrolyte interphase (SEI) in lithium-ion batteries. ACS Appl. Mater. Interfaces 7, 20004–20011.

12. Zhang, Y., Du, N., and Yang, D. (2019). Designing superior solid electrolyte interfaces on silicon anodes for high-performance lithium-ion batteries. Nanoscale 11, 19086–19104.

13. Feng, K., Li, M., Liu, W., Kashkooli, A.G., Xiao, X., Cai, M., and Chen, Z. (2018). Silicon-Based Anodes for Lithium-Ion Batteries: From Fundamentals to Practical Applications. Small 14, 1702737.

14. Veith, G.M., Doucet, M., Sacci, R.L., Vacaliuc, B., Baldwin, J.K., and Browning, J.F. (2017). Determination of the solid electrolyte interphase structure grown on a silicon electrode using a fluoroethylene carbonate additive. Sci. Rep. 7, 6326.

15. Nanda, J., Yang, G., Hou, T., Voylov, D.N., Li, X., Ruther, R.E., Naguib, M., Persson, K., Veith, G.M., and Sokolov, A.P. (2019). Unraveling the Nanoscale Heterogeneity of Solid Electrolyte Interphase Using Tip-Enhanced Raman Spectroscopy. Joule 3, 2001–2019.

16. Stetson, C., Yoon, T., Coyle, J., Nemeth, W., Young, M., Norman, A., Pylypenko, S., Ban, C., Jiang, C.-S., Al-Jassim, M., and Burrell, A. (2019). Three-dimensional electronic resistivity mapping of solid electrolyte interphase on Si anode materials. Nano Energy 55, 477–485.

17. Rehnlund, D., Lindgren, F., Böhme, S., Nordh, T., Zou, Y., Pettersson, J., Bexell, U., Boman, M., Edström, K., and Nyholm, L. (2017). Lithium trapping in alloy forming electrodes and current collectors for lithium based batteries. Energy Environ. Sci. 10, 1350–1357.

18. Michan, A.L., Divitini, G., Pell, A.J., Leskes, M., Ducati, C., and Grey, C.P. (2016). Solid electrolyte interphase growth and capacity loss in silicon electrodes. J. Am. Chem. Soc. 138, 7918–7931.

19. Zhao, X., and Lehto, V.-P. (2021). Challenges and prospects of nanosized silicon anodes in lithium-ion batteries. Nanotechnology 32, 042002.

20. Wu, Q., Shi, B., Bareño, J., Liu, Y., Maroni, V.A., Zhai, D., Dees, D.W., and Lu, W. (2018). Investigations of Si Thin Films as Anode of

Lithium-Ion Batteries. ACS Appl. Mater. Interfaces 10, 3487–3494.

21. Reyes Jiménez, A., Nölle, R., Wagner, R., Hüsker, J., Kolek, M., Schmuch, R., Winter, M., and Placke, T. (2018). A step towards understanding the beneficial influence of a LIPON-based artificial SEI on silicon thin film anodes in lithium-ion batteries. Nanoscale 10, 2128–2137.

22. Wang, J.W., He, Y., Fan, F., Liu, X.H., Xia, S., Liu, Y., Harris, C.T., Li, H., Huang, J.Y., Mao, S.X., and Zhu, T. (2013). Two-phase electrochemical lithiation in amorphous silicon. Nano Lett. 13, 709–715.

23. Fang, C., Li, J., Zhang, M., Zhang, Y., Yang, F., Lee, J.Z., Lee, M.H., Alvarado, J., Schroeder, M.A., Yang, Y., et al. (2019). Quantifying inactive lithium in lithium metal batteries. Nature 572, 511–515.

24. Zhao, L., Dvorak, D.J., and Obrovac, M.N. (2016). Layered amorphous silicon as negative electrodes in lithium-ion batteries. J. Power Sources 332, 290–298.

25. Erogbogbo, F., Lin, T., Tucciarone, P.M., LaJoie, K.M., Lai, L., Patki, G.D., Prasad, P.N., and Swihart, M.T. (2013). On-demand hydrogen generation using nanosilicon: splitting water without light, heat, or electricity. Nano Lett. 13, 451–456.

26. Henssge, A., Acker, J., and Müller, C. (2006). Titrimetric determination of silicon dissolved in concentrated HF-HNO3-etching solutions. Talanta 68, 581–585.

27. Huang, W., Wang, J., Braun, M.R., Zhang, Z., Li, Y., Boyle, D.T., McIntyre, P.C., and Cui, Y. (2019). Dynamic structure and chemistry of the silicon solid-electrolyte interphase visualized by cryogenic electron microscopy. Matter 1, 1232–1245.

28. Farley, T., Hayes, W., Hull, S., Hutchings, M., and Vrtis, M. (1991). Investigation of thermally induced Li+ ion disorder in Li2O using neutron diffraction. J. Condens. Matter Physiol. 3, 4761.

29. Idemoto, Y., Richardson, J.W., Jr., Koura, N., Kohara, S., and Loong, C.-K. (1998). Crystal structure of (LixK1−x)2CO3 (x = 0, 0.43, 0.5, 0.62, 1) by neutron powder diffraction analysis. J. Phys. Chem. Solids 59, 363–376.

30. Recker, K., Wallrafen, F., and Dupre, K. (1988). Directional solidification of the LiF-LiBaF3 eutectic. Naturwissenschaften 75, 156–157.

31. Gu, M., Wang, Z., Connell, J.G., Perea, D.E., Lauhon, L.J., Gao, F., and Wang, C. (2013). Electronic origin for the phase transition from amorphous Li(x)Si to crystalline Li15Si4. ACS Nano 7, 6303–6309.

32. Cheng, D., Wynn, T.A., Wang, X., Wang, S., Zhang, M., Shimizu, R., Bai, S., Nguyen, H., Fang, C., Kim, M.-C., and Li, W. (2020). Unveiling the Stable Nature of the Solid Electrolyte Interphase between Lithium Metal and LiPON via Cryogenic Electron Microscopy. Joule 4, 2484–2500.